Application of the multi-site ion exchanger model to the sorption of Sr and Cs on natural clayey sandstone

Aubéry Wissocq, Catherine Beaucaire, Christelle Latrille

Application of the multi-site ion exchanger model to the sorption of Sr and Cs on natural clayey sandstone

Aubéry Wissocq[a]*, Catherine Beaucaire[a], Christelle Latrille[a]

[a]Den-Service d'Etude du Comportement des Radionucléides (SECR), CEA, Université Paris-Saclay, F-91191, Gif-sur-Yvette, France

Corresponding author. Tel.: +33-(0)169-087-013; fax: +33-(0)169-083-242.
E-mail address: aubery.wissocq@cea.fr

Abstract

To ensure the environmental monitoring of nuclear sites, sorption models enabling the prediction of contaminant migration (such as ^{90}Sr and ^{137}Cs) in soils, sediments and aquifers need to be developed. This paper aims 1) at developing a database containing the sorption properties of the pure mineral phases commonly encountered in natural environments and 2) at using this database in a multi-site ion exchange model to be applied on natural sediments. In addition to some raw adsorption data issued from literature, different sorption experiments of Sr and Cs, on pure illite and smectite, in competition with calcium were carried out, as a function of pH and as well as concentrations of Sr and Cs. These sorption data were interpreted using a multi-site ion-exchange model and contributed to the elaboration of a thermodynamic database gathering the retention properties of illite and smectite (site capacities and selectivity coefficients) towards Cs^+, Sr^{2+}, H^+ and Ca^{2+}. A multi-site ion exchange model based on the mixture of pure mineral phases (illite and smectite) was successfully applied to simulate the Sr and Cs behavior in a natural clayey sandstone, indicating that the additivity of retention properties of the minerals constituting the sediment can be verified.

Keywords: illite; smectite; strontium; cesium; sorption; ion exchange model

1. Introduction

Since the arrival of the nuclear industry in the 1940s, radionuclides have been introduced in the environment whether by nuclear accidents, such as Chernobyl or more recently Fukushima, by

weapons testing or by nuclear waste repositories. ^{90}Sr and ^{137}Cs are fission products of uranium and plutonium used in the reactors and are present in nuclear waste. They hold our attention because of their long half-life (29 y and 30 y) and their solubilities which cause a release in the environment. Therefore, to evaluate the environmental impact of nuclear sites, migration processes of ^{90}Sr and ^{137}Cs in soils, sediments and aquifers have to be understood and well predicted.

The migration of ^{90}Sr and ^{137}Cs in natural environments is partly governed by sorption phenomena on minerals, especially clay minerals. Indeed, due to their negative surface charges (permanent charge, silanol, aluminol, frayed-edge…) compensated by cations, clay minerals are particularly known to present different sorption site types. Based on these exchange cation properties, many sorption models have been developed to interpret sorption of contaminants in a complex mineralogical assemblage. Most of them are empirical models, unable to take into account the variations in chemical conditions occurring in natural environments, especially when it comes to the sorption of trace elements competing with major cations in solution (El Aamrani et al., 2002; Kurosawa et al., 2006; Vandenhove et al., 2007).

Thermodynamic models, based on mass action laws, considering sorption processes as ion exchange (Beek et al., 1979) or surface complexation phenomena (Bolt et al., 1991), are more appropriate in these contexts. Regardless of the model chosen to simulate sorption data for natural materials, many authors have preferred a generalized composite approach to a component additivity approach. Effectively, this latter approach requires a database compiling the sorption properties of all phases involved in a mineralogical assemblage. The lack of sorption data for pure minerals is usually highlighted to argue the discrepancy between modeling outcomes and experimental data (Voegelin et al., 2000; Vulava et al., 2000; 2002; Steefel et al., 2003; Tertre et al., 2008).

Models based on a generalized composite approach include input parameters (i.e., the composition of surface coatings, site capacities, surfaces site types…) related to a selected global material under a certain chemical condition, that cannot be extrapolated to different natural environments. In the case of surface complexation, the component additivity approach to predict sorption by complex substrates remains difficult to demonstrate. Some fitting parameters (in particular reactive surface areas) are still required despite recent modeling advances (Davis et al., 1998; 2004;

Payne et al., 2004; Landry et al., 2009, Schaller et al., 2009; Reich et al., 2010; Dong et al., 2012). However, an ion-exchange model based on the multi-site ion-exchanger formalism adapted by Ly et al. (1991) combines the sorption properties of pure mineral phases. It can successfully predict Cs, Am and Se sorption on several montmorillonite and goethite or calcite mixtures (Peynet, 2003). More recently, it was applied to more complex mineralogical assemblages such as natural soil and sediments. Zn sorption in trace concentrations, modeled using the component additivity approach was found to be in good agreement with batch data acquired for global sediments (Tertre et al., 2009).

This study aims at assessing the ability of the latter approach to predict Sr and Cs sorption on a natural clayey sandstone. For this purpose, it was assumed that Sr and Cs sorption processes are due to illite and smectite, acting as the main reactive minerals of this clay mineral assemblage. In this physico-chemical context, Ca is identified as the major exchangeable cation. Consequently, it is referred to as the major competitor to trace elements in solution.

To model Cs and Sr sorption on the selected clayey sandstone, a database has to compile the respective illite and smectite sorption properties towards Sr, Cs and Ca, interpreted with the multi-site ion-exchanger formalism. To create this database, a review of the data available in the literature was carried out and is discussed throughout this manuscript. There was particularly a significant discrepancy between these different sorption data sets and some lacks concerning Sr and Cs sorption in competition with Ca. Faced with this disparity, new sorption data describing illite and smectite sorption properties towards Sr, Cs and Ca are presented in this study. The ability of this model to predict Sr and Cs sorption on the clayey sandstone, based on an additivity approach was then assessed by comparing modeling outcomes with experimental results.

2. Methodology

This part presents the formalism developed in the multi-site ion exchanger model, the methodology to elaborate the database and the additivity approach used to model sorption on complex mineralogical assemblages. The formalism used in this study was previously detailed by the following

authors (Motellier et al., 2003; Jacquier et al., 2004; Tertre et al., 2009; Savoye et al., 2012; Reinoso-Maset and Ly, 2014).

Clay minerals are known to support various sorption site types, such as planar sites associated to the permanent negative charge resulting from isomorphous substitution of lattice cations, and surface hydroxyl-groups able to protonate or deprotonate depending on pH. In the present ion-exchange model, clay minerals are defined as an exchanger with different negatively charged sorption sites, named X_i, contributing to the intrinsic surface reactivity (Reinoso and Ly, 2016). Considering the ion-exchange between a cation M^{m+} and H^+ taken as reference, the reaction associated to sorption site X_i is expressed by the following equilibrium (Eq.1):

$$m\{(X_i^-) - H^+\} + M^{m+} = \{(X_i^-)_m - M^{m+}\} + mH^+ \qquad (1)$$

associated with an equilibrium constant:

$$K^{i*}_{mH^+/M^{m+}} = \frac{[(X_i^-)_m - M^{m+}]\,[H^+]^m (\gamma_{H^+})^m}{[(X_i^-) - H^+]^m\,[M^{m+}]\;\gamma_{M^{m+}}} \qquad (2)$$

where K^* is the corrected selectivity coefficient, *i* is the type of sorption site, [ ] is the concentration of species in solution (mol/L) or sorbed species (mol/kg of dry solid) and γ is the activity coefficient of species in solution. The activity coefficients of the aqueous species are calculated with the Davies equation (Davies, 1938). The activity coefficients of the adsorbed species are unknown, but their ratio is expected to be constant.

The capacity of major sorption site types are generally deduced from saturation curves expressed in terms of the concentration of adsorbed species (mol/kg of solid) over a wide range of pH (2 to 11). These curves are acquired for each major cation of interest, on homo-ionic clay minerals, and under chemical conditions leading to the saturation of site capacities, i.e., with a slight excess of cation in solution relative to its maximum uptake by the solid. Each site exchange capacity is expressed by a plateau corresponding to an exchange reaction at equilibrium between cation and proton. Thus, for each X_i site we determine the site capacity CE_i.

The site capacity CE_i is the sum of the concentrations of adsorbed species on an X_i site:

$$CE_i = [X_i^- - H^+] + m[(X_i^-)_m - M^{m+}] \qquad (3)$$

In case of multi-sites, the sum of CE_i has to be equal to the cation exchange capacity (CEC) of the studied sorbent. Combining the equations (2) and (3), the concentration of sorbed M^{m+} can be expressed by the relations (4) and (5) for monovalent and divalent cations, respectively:

$$[X_i^- - M^+] = \frac{CE_i}{1+\frac{1}{K^{*i}_{H^+/M^+}\ \gamma_{M^+}\ [M^+]}10^{-pH}} \qquad (4)$$

$$[(X_i^-)_2 - M^{2+}] = \frac{CE_i}{2} + \frac{1}{8}\frac{10^{-2pH}}{K^{*i}_{2H^+/M^{2+}}\ \gamma_{M^{2+}}\ [M^{2+}]} -$$

$$\frac{1}{8}\sqrt{\left(\frac{10^{-2pH}}{K^{*i}_{2H^+/M^{2+}}\ \gamma_{M^{2+}}\ [M^{2+}]}\right)^2 + 8CE_i\frac{10^{-2pH}}{K^{*i}_{2H^+/M^{2+}}\ \gamma_{M^{2+}}\ [M^{2+}]}} \qquad (5)$$

The selectivity coefficients $K^{i*}_{mH^+/M^{m+}}$ are determined by fitting equation (4) or (5) to an experimental saturation curve using each previously determined site capacity CE_i (as seen in Fig. 1). Sorption site capacities quantified for each sorbent are assumed to be constant regardless of the two cations in competition on the surface sites. Their values issued from major cation saturation curves (Ca, Na, K, Mg) remain the same to handle trace element sorption.

In the present study, with consideration taken to trace elements (Sr^{2+} or Cs^+), competing with both H^+ and Ca^{2+}, two additional ion exchange equilibria between Sr^{2+} or Cs^+ with H^+ must be taken into account for each site X_i. The adsorbed Sr^{2+} or Cs^+ concentrations are respectively given by equations (6) and (7). Under our experimental conditions, cations are predominantly in free form.

$$[(X_i^-)_2 - Sr^{2+}] = \frac{1}{16}\frac{(\sqrt{8CE_i\ (AB+1)+B}-\sqrt{B})^2}{(AB+1)^2} \qquad (6)$$

with $A = \frac{K^{i*}_{2H^+/Ca^{2+}}\ \gamma_{Ca^{2+}}\ [Ca^{2+}]}{10^{-2pH}}$ and $B = \frac{10^{-2pH}}{K^{i*}_{2H^+/Sr^{2+}}\ \gamma_{Sr^{2+}}\ [Sr^{2+}]}$

and

$$[(X_i^-) - Cs^+] = \frac{-(C+1)+\sqrt{(C+1)^2+8CE_iC^2D}}{4C^2D} \qquad (7)$$

with $C = \frac{10^{-pH}}{K^{i*}_{H^+/Cs^+}\ \gamma_{Cs^+}\ [Cs^+]}$ and $D = \frac{K^{i*}_{2H^+/Ca^{2+}}\ \gamma_{Ca^{2+}}\ [Ca^{2+}]}{10^{-2pH}}$

To apply this sorption model to a mineralogical assemblage, we used a component additivity approach. This implies that the site capacities of the mineralogical assemblage are the sum of the site capacities of each mineral component weighted by their relative abundance in the assemblage. In our mineralogical system, illite and smectite mainly govern the clayey sandstone sorption properties by ion-exchange processes. Consequently, the clayey sandstone site capacity [X^-], equal to its CEC, can be expressed by equation (8):

$$[Xi^-] = CEC_{sandstone} = \sum_i (x_{illite} * CE_{i_{illite}} + x_{smectite} * CE_{i_{smectite}}) \quad (8)$$

where x_{illite} and $x_{smectite}$ are the illite and smectite abundance in the clayey sandstone and $CE_{i_{illite}}$ and $CE_{i_{smectite}}$ are respectively the illite and smectite X_i^- site capacity.

Selectivity coefficients in the mineralogical assemblage are those determined on each site of pure illite and smectite. This multi-site ion exchanger model can be implemented in PHREEQC code using the EXCHANGE data block. Corrected selectivity coefficients obtained from the multi-site ion exchanger formalism have to be converted into the Gaines-Thomas formalism expected by PHREEQC.

3. Materials and methods

3.1. Illite, smectite and clayey sandstone preparation

The pure clay minerals, illite and smectite, selected for this study, have been extensively studied as reflected by the large amount of literature about them, and they have been used as reference

minerals. The illite is an “Illite du Puy” extracted from the Oligocene geological formation located in the region of Le Puy-en-Velay (Haute-Loire, France). The mineral composition can vary from pure illite to illite with impurities such as kaolinite, carbonates, quartz and feldspars (Gabis, 1958; Van Olphen and Fripiat, 1979; Gorgeon 1994; and Poinssot et al., 1999). The smectite used is a montmorillonite SWy-2 obtained from the Wyoming bentonite MX80 which contains accessory minerals such as quartz, carbonates, feldspars, pyrite and micas or illite (Gorgeon 1994; Nolin 1997; Sauzéat et al., 2000; Guillaume 2002; Michot et al., 2004). Both the studied illite and smectite were initially purified by dissolving carbonate in 0.1M HCl solution and by sieving at 25 µm the resulting suspension to remove accessory minerals. The purification treatment for these fractions was controlled by XRD analysis. Moreover, no significant illite trace was detected in the smectite by XRD.

The clayey sandstone (CS) used in this study was collected at 31 meters depth in the Miocene geological formation hosting the groundwater table located below the Cadarache nuclear research center (France). CS is mainly composed of quartz (75 wt.%), clay minerals (20 wt.%), carbonates (2.5 wt.%) and iron oxides (2 wt.%). Sr and Cs sorption experiments were performed on the < 25 µm fraction isolated from the global CS, slightly crushed manually in an agate mortar and wet-sieved at 25 µm. In this way, quartz, not involved in sorption processes, was removed to focus on Sr and Cs sorption onto clay minerals. An XRD mineralogical quantification of this < 25 µm fraction revealed about 37 wt.% kaolinite, 27 wt.% illite, 26 wt.% smectite, 2 wt.% chlorite, approximately 19 wt.% quartz and goethite and no carbonates. Under our experimental chemical conditions (pH 6.5), goethite remained positively charged and could be neglected in the complete ion exchange process. Moreover, chlorite and kaolinite exchange capacities were lower than those of illite and smectite. Weighted by their relative abundance, chlorite and kaolinite contributed to the material exchange capacity at a level equivalent to the CEC measurement uncertainty (0.020 eq/kg, 6.3% of CEC material). Consequently, smectite and illite were assumed to govern the sorption processes on this clayey sandstone.

Since Ca was the major exchangeable cation of the clayey sandstone; illite, smectite and CS were conditioned under a homo-ionic Ca-form in order to simplify the material reactivities to exchange reactions with Ca^{2+} and H^{+}. To this end, illite and smectite were dispersed in 1M $CaCl_2$ with

a 1:10 solid/solution ratio, shaken for 24 h on an orbital shaker and centrifuged to replace the supernatant by a 1M $CaCl_2$ solution. These operations were repeated 5 times. Two similar operations were successively realized with 0.1M $CaCl_2$ and finally ethanol to eliminate residual salt. After centrifugation, both conditioned materials were left to air-dry for 2 days. The CS < 25 µm fraction was conditioned only in 0.1M $CaCl_2$ solution with a 1:10 solid/solution ratio. The following conditioning steps were the same as those applied to illite and smectite.

CEC measurements were performed by K/Cs cation exchange on these three conditioned materials. Firstly the three materials were saturated with K at pH 9. Secondly, K was exchanged with Cs and the concentration of released K was analyzed by ionic chromatography. The conditioned illite CEC was estimated at 0.240 ± 0.008 eq/kg of dry solid which was consistent with the current CEC values measured on purified illite du Puy, i.e., 0.248 eq/kg on a < 80 µm fraction (Gorgeon, 1994), 0.232 eq/kg for Gaucher (1998) and 0.225 eq/kg for Baeyens and Bradbury (2004) on a < 63 µm fraction.

The conditioned smectite CEC was measured at 0.898 ± 0.037 eq/kg, which was consistent with the current CEC values of Wyoming montmorillonite (0.875 eq/kg on a < 2 µm fraction (Sauzéat et al. 2000, Guillaume 2002) 0.910 eq/kg on a < 0.5 µm fraction (Michot et al., 2004) and 0.887 eq/kg for Nolin (1997)). The CEC value obtained on the conditioned < 25 µm fraction of CS was 0.326 ± 0.020 eq/kg, which corresponded well with the relative abundances of kaolinite, illite and smectite.

3.2. Sorption Experiments.

Despite the abundance of Ca in the natural environment, no Ca sorption data are available on pure illite in the literature. Only one Sr sorption dataset obtained on Ca-illite (Wahlberg et al., 1965) was acquired as a function of concentration, at fixed pH. Therefore, for the requirement of the present study, it appeared necessary to address this lack of sorption data. Wissocq et al. (2017) proposed a new Sr sorption experiment depending on pH on pure Ca-illite, in addition to a Ca saturation curve on illite

du Puy. However, due to the discrepancy between CEC of the studied illite du Puy and Wahlberg's illite, more data are required.

In addition, there is also Sr and Cs sorption data on Ca-smectite acquired by Wahlberg et al. (1965), Wahlberg and Fishman (1962) and Missana et al. (2014a). However, these sorption data were acquired only as a function of the concentration at fixed pH.

In complement to the collected sorption datasets on Ca-illite and Ca-smectite available in the literature, five sorption experiments were carried out in this study in order to consolidate our database. They concerned: (1) a Sr sorption isotherm on Ca-illite vs. the Sr concentration, in complement to the isotherm of Wissocq et al. (2017) performed over a wide range of pH (pH 3 to 12); (2) four Sr and Cs sorption isotherms on Ca-smectite vs. concentration and pH. Moreover, Sr and Cs sorption isotherms vs. concentration were performed on the < 25 µm fraction of conditioned CS material. All sorption isotherms were performed at identical ionic strengths, I = 0.03M, in a $CaCl_2$ solution.

Batch sorption experiments were conducted in polycarbonate centrifuge tubes filled with 0.11 g of dried Ca-conditioned material dispersed in 5 ml of 0.01M $CaCl_2$ solution (i.e., with a solid/liquid ratio ~ 0.02 g/l). All solutions used for these isotherms were de-aerated by bubbling N_2 gas through them to avoid $CaCO_3$ precipitates in suspensions at basic pH. Each batch suspension was spiked with ^{85}Sr or ^{134}Cs by adding only 50 µl of a source ($^{85}SrCl_2$ or $^{134}CsCl$ in HCl 0.1M) containing an activity of 70000 Bq/ml. The initial labeled Sr and Cs concentration introduced in each tube was around 10^{-7} M. Sr and Cs adsorption experiments on illite, smectite and CS material over a concentration range were carried out, at fixed pH for each batch as well as at a fixed background electrolyte concentration. In addition to radiotracer (10^{-7}M), stable isotopes ($SrCl_2$ and CsCl solutions, Merck) were added to achieve a solute concentration ranging between 10^{-1} and 10^{-8}M at equilibrium.

In the illite and CS material, the pH was naturally buffered around 6.3 and 6.4, respectively, during all experimental steps. In the case of Ca-smectite, Sr and Cs sorption isotherms were measured at a fixed pH of 7.5 (pH naturally buffered) and 4, respectively. The latter acidic pH was imposed by H^+ added with the radiotracer solution and not compensated.

For Sr and Cs sorption experiments on Ca-smectite over a pH range, the pH was adjusted in each centrifuge tube to achieve final pH values ranging between 2 and 12 by using HNO_3^- (10^{-1}-10^{-3}M) or $Ca(OH)_2$ (10^{-2}-10^{-4}M) solutions. The suspensions were shaken for a few hours to favor pH equilibration before adding radiotracers. For each isotherm, final suspensions in contact with the different solids were shaken during 6 days. The equilibrium solution of different batches was then analyzed. The supernatant was separated from the solid by ultracentrifugation for 30 min at 33000 g (Beckman Optima LE-80K Ultracentrifuge). These centrifugation conditions ensured the > 0.2 µm separation from solution. The supernatants were totally extracted from the centrifuge tubes and kept for electrolyte concentration analysis, counting of radioelement activity and to check the pH at equilibrium.

Chemical analyses of Ca were carried out by ionic chromatography (standards Chem-Lab) whereas Sr and Cs were analyzed by ICP-MS (standards Plasma CAL). The measurement uncertainties were 2%. The radioactivity of 1 ml supernatant was measured by gamma counting (Perkin Elmer Wizard 3). pH values were determined using a combined glass pH electrode (Mettler Toledo) equipped with an Ag/AgCl reference electrode. The electrode was calibrated with buffer solutions at pH 4.01, 7 and 12.

Sr and Cs sorption reversibility was also studied on experiments performed on the three materials. As for the reversibility, we attempted to verify that the desorption reaction at equilibrium maintained the same solute distribution between solid and solution as the sorption reaction under the same conditions. At the end of the sorption experiments, the supernatants were entirely extracted and replaced with 5 ml of 0.01M $CaCl_2$ solution. When necessary, the pH was adjusted in each centrifuge tube to attain the initial pH value imposed in the sorption experiments. The suspensions were then shaken during 6 days after which they were centrifuged according to the sorption experiment protocol. 1 ml of supernatants was sampled in each centrifuge tube in order to count the released activities in solution and the remaining supernatant was kept for analysis of the solute concentrations at equilibrium.

The distribution coefficients between solid and solution K_d (L/Kg) were calculated for Sr and Cs on each sorption experiment following the relation (9):

$$K_d = \frac{\overline{[Me]}}{[Me]} = \left(\frac{A_0}{A} - 1\right)\frac{V}{m} \qquad (9)$$

where $\overline{[Me]}$ and $[Me]$ are respectively the total concentration at equilibrium of adsorbed Me and the total concentration of Me in solution, A_0 is the initial solution activity, A the activity in solution at equilibrium, m the solid dry mass and V the total volume of solution.

Sr and Cs K_d for the desorption experiment were calculated by the relation (10):

$$K_{d\,des} = \left(\frac{A_0 - A}{A_{des}} - 1\right)\frac{V}{m} \qquad (10)$$

where A_{des} is the activity at equilibrium in solution after desorption.

The uncertainties with regard to the K_d value were calculated by the uncertainties propagation law. For each batch tube were calculated σ_{K_d}, the standard deviation of the K_d (dependent on different variables x_i) by the following Eq 11:

$$\sigma_{K_d}^2 = \sum_i \left(\frac{\partial K_d}{\partial x_i}\right)^2 \sigma_i^2 + 2\sum_i \sum_j \frac{\partial K_d}{\partial x_i}\frac{\partial K_d}{\partial x_j}\sigma_{ij} \qquad (11)$$

where σ_i^2 is the variance of the x_i variable and σ_{ij} is the covariance of the x_i and x_j variables. If x_i and x_j variables are independent, the covariance is zero.

4. Results and discussion

4.1. Constituting a database compiling sorption parameters of illite and smectite

In order to apply the additivity model to predict Cs and Sr sorption on a natural composite material, a database compiling sorption parameters of illite and smectite had to be created. According to the multi-site ion exchange formalism, sorption parameters of pure phases (illite and smectite) were

expressed by site capacities (eq/kg) and the selectivity coefficients associated with each sorption site, $K^{i*}_{2H+/Ca2+}$, $K^{i*}_{2H+/Sr2+}$ and $K^{i*}_{H+/Cs+}$.

Firstly, we determined sorption site capacities of each pure mineral and their specific sorption affinity towards Ca^{2+}. Secondly, Cs and Sr behaviors onto illite and smectite competing with Ca^{2+} were studied.

4.1.1. High-capacity sites and their respective selectivity coefficients

In saturation curves (see §2), the evolution of adsorbed cation concentration (eq/kg) with pH depicts the progressive replacement of protons adsorbed on sorption sites by the free cation. The saturation of the different sorption sites is evidenced by a successive plateau, as presented in Fig. 1.

Concerning the smectite, sorption properties toward major cations have been widely studied in the literature (Peynet, 2003; Gorgeon, 1994; Gaucher, 1998; Nolin, 1997; Tournassat et al., 2004) and important discrepancies were found between the sorption datasets. A compilation of these datasets allowed establishing a sorption properties database for major cations. For the purpose of this study, we only used Ca sorption datasets of Peynet (2003) on a Ca-smectite for which the CEC is close to ours (Fig. 1). A Na saturation curve obtained on smectite by Nolin (1997) describes the smectite ion-exchanger with three major sorption sites (0.387, 0.361 and 0.139 eq/kg). These former data had already been used by Tertre et al. (2009) for the study of Zn sorption and recently discussed in Robin et al. (2015).

Selectivity coefficients $K^{i*}_{2H+/Ca2+}$ were fitted to the Ca saturation curve according to relation (5). However, in the case of Ca^{2+}, as can be seen in Fig. 1, the first site was oversaturated from pH 2.0. Thus, the selectivity coefficients $K^{i*}_{2H+/Ca2+}$ determined on this first Xe site was difficult to constrain. Supplementary Na/Ca exchange curves were thus necessary in order to accurately constrain this selectivity coefficient. The three sorption curves used to determine the corrected selectivity coefficients $K^{i*}_{2H+/Ca2+}$ were therefore the Ca saturation curve (Fig. 1) and the Ca sorption curves vs. the Ca concentration at pH 6.4 and 10.2 on Na-smectite (Peynet, 2003; Appendix2). Site capacities proposed by Nolin (1997) and $K^{i*}_{H+/Na+}$ selectivity coefficients proposed by Siroux et al. (2017) were

used to adjust the $K^{i*}_{2H+/Ca2+}$ selectivity coefficients on the three curves simultaneously (Table A1, Appendix 2).

According to the Ca saturation curve of illite (Wissocq et al., 2017), illite can be described by three sorption sites for which the site capacities are 0.131, 0.043 and 0.074 eq/kg (see Fig. A1). The different site capacities and the associated selectivity coefficients related to the exchange of Ca^{2+} versus H^+ for illite and smectite are listed in Table 1.

4.1.2. Identifying low-capacity sites and selectivity coefficients of trace elements

The low-capacity sites, for which the capacity is generally inferior to 0.5 % of the total exchange capacity (Brouwer et al., 1983; Peynet, 2003; Bradbury and Baeyens, 2000; Missana et al., 2014a), cannot be evidenced on the saturation curves. This kind of site, frequently named “frayed-edge site” in the literature, is located at the edge of the interlayer space where it expands with the weathering of the mineral (Jackson, 1963; Sawhney, 1972). These low-capacity sites have previously been recognized to be involved in trace element sorption on clay minerals and to act principally at low concentration (Sawhney, 1972; Brouwer et al., 1983; Comans et al., 1991; Baeyens and Bradbury, 1997; Poinssot et al., 1999; Peynet, 2003; Missana et al., 2004; Jacquier et al., 2004; Tertre et al., 2009). They have been evidenced on sorption isotherms vs. concentration. We have successively examined cases of illite and smectite.

4.1.2.1 Illite

In this study, in complement to the Sr isotherm vs. pH (Fig. A2) from Wissocq et al (2017), a Sr sorption isotherm on Ca-illite vs. the Sr concentration is presented at pH 6.5 (Fig.2). This curve shows a decrease of $\log(K_d)$ values from 1.30 to 0.70 L/kg which can be interpreted as site saturation. The K_d desorption curve could be superimposed on the K_d sorption curve at identical experimental conditions indicating that the sorption reaction was reversible. These data were compared with those of Wahlberg et al (1965). Even though the shapes of the curves were similar, the K_d values obtained in our study were higher than those of Walhberg et al. (1965) for the same ionic strength (0.03M) and a

supposedly similar pH (pH 7). This difference was probably due to the lower CEC of the Fithian illite they used (i.e., 0.150 eq/kg).

In Fig. 6, the concentrations of adsorbed Sr are plotted versus the Sr concentrations in solution at equilibrium. We can observe a slight slope rupture indicating a possible saturation of the low-capacity site, for an adsorbed concentration around 0.003 eq/kg (-2.5 on the log scale). Even low capacity sites on illite are generally recognized for elements such as Cs or Zn (Poinssot et al., 1999; Altmann et al., 2014): they have never been observed for Sr before this study. It is generally admitted that, contrary to Cs, Sr is characterized by a linear isotherm (adsorbed concentration linear vs. concentration at equilibrium) (Rafferty et al., 1981).

The Cs sorption isotherm on Ca-illite vs. the concentration (Fig 3), as obtained by Missana et al. (2014b), helps determine the corrected selectivity coefficients $K^{i*}_{H+/Cs+}$. Therefore, it appears necessary to take into account a fourth site, in addition to the three major ones previously identified (§ 4.1.1), to match the high K_d(Cs) values at Cs concentrations below 10^{-6} M. Even more than for Sr, the Cs curves (Fig. 3 and 6) highlighted a low-capacity site with high affinity for Cs as already observed on illite (Sawhney, 1972; Brouwer et al., 1983).

The Sr (Wissocq et al., 2017; this study) and Cs (Missana et al., 2014b) sorption curves on Ca-illite were interpreted with the multi-site ion exchange formalism. Selectivity coefficients $K^{i*}_{2H+/Sr2}+$ and $K^{i*}_{H+/Cs}+$ were obtained by fitting the theoretical sorption equations (6) and (7) to the experimental results, keeping the three high-capacity sites Xa, Xb, Xc fixed as well as their associated, previously determined, selectivity coefficients $K^{i*}_{2H+/Ca2+}$.

Considering that site capacity is an intrinsic property for clay minerals, the low-capacity site Xh should remain constant regardless of the considered element. Therefore, the fitting method consisted in simultaneously optimizing the selectivity coefficients from both Sr and Cs sorption curves by non-linear regression using an Excel solver. The concentration of the low-capacity site (Xh) and the selectivity coefficients $K^{i*}_{2H+/Ca2}+$ associated with this site were also adjusted. Uncertainties with

regard to the selectivity coefficients estimated by the Excel solver were calculated using the Excel macro SolverAid.

The corrected selectivity coefficients obtained for illite are listed in Table 1. The Xh value was adjusted at 0.001 eq/kg. This value was slightly lower than that found by only adjustment of Sr sorption curves (0.005 eq/kg in Wissocq et al., 2017), and that used by Altmann et al. (2014) to model Zn sorption on Na-illite (0.002 eq/kg). Lower values were also found by Poinssot et al. (1999): i.e., 0.0005 eq/kg for Cs sorption on Na-illite, which is close to that determined by Missana et al. (2014b) for Cs sorption on Ca-illite (i.e.0.0003 eq/kg). Such differences evidence the difficulties to constrain this low site capacity with good accuracy and the impossibility to assign it to the mineral structure. However, these differences are not surprising given the natural high variability observed in a same group of clay minerals, and the nature of this kind of site generally described as resulting from the alteration of edge sites.

It is therefore possible to model Ca, Sr and Cs sorption on Ca-illite with only one set of retention parameters. Note that for Cs, the contributions of sites b and c are too low to be accurately estimated.

4.1.2.2 Smectite

Sr and Cs sorption and desorption data on Ca-smectite obtained in this study are presented in Fig. 4 (a) and (b), 5 (a) and (b) and were interpreted with the same approach and formalism as previously used. Fig 4(a) and 5(a) show that Sr and Cs sorption on Ca-smectite was practically constant between pH 4 and 10. Modeling results suggest that the high-capacity site Xe was already saturated at pH < 4. For both elements, desorption curves vs. pH and concentration were superimposed to the sorption curves suggesting the reversibility of the sorption reactions. The adsorbed Cs sorption curves vs. concentration (Fig. 6) revealed a slight break in the slope which suggests that at low concentration (below 10^{-5} M), a low-capacity site was already saturated. This site capacity could be estimated at about 0.0003 eq/kg (around -3.5 on Fig. 6) and its contribution was required to match the Cs sorption curves vs. concentration (Fig. 5b). However, the contribution of such a site type in Sr sorption on Ca-smectite could not be clearly evidenced. The contribution of low-capacity sites on Ca-smectite is generally recognized for Zn (Baeyens and Bradbury, 1997; Bradbury and Baeyens, 1999)

but has been observed only once for Cs by Peynet (2003). Missana et al. (2014a) also found a low-capacity site on Ca-smectite but this one was attributed to the presence of illite in a mixture with smectite.

The previous data obtained by Wahlberg et al. (1965) and Wahlberg and Fishman (1962), K_d(Sr) on Ca-smectite (from Burns, Mississipi) are very similar to those presented in this study (Fig. 4b) despite the fact that the CEC value (1.300 eq/kg) was higher than that for montmorillonite SWy-2. In the case of Cs (Fig. 5b), the K_d(Cs) values obtained by Walhberg and Fishman (1962) on Ca-smectite at the same ionic strength but at higher pH (i.e., 7.0) were slightly higher (by a 0.5 log unit). The results by Missana et al. (2014a) obtained at higher ionic strength (i.e., 0.1M) were ten times higher than ours. However, as previously observed, K_d(Cs) on Ca-smectite appeared to be relatively constant between pH 4 and 7, indicating that the higher Cs sorption observed by Wahlberg and Fishman (1962) was likely due to the different nature of the smectite used in their experiment.

The fourth site Xj capacity calculated to match the Cs sorption curves (Fig. 5) was estimated at 0.0001 eq/kg, similar to the results by Missana et al. (2014a) estimated at 0.00012 eq/kg, and slightly lower than Peynet's value (2003) at 0.0005 eq/kg studying Cs sorption on Na-montmorillonite or those of Bradbury and Baeyens (1999) estimated at 0.002 eq/kg, through a Zn sorption experiment on a Ca-montmorillonite.

The corrected selectivity coefficients obtained for smectite are listed in Table 1. As for illite, it was possible to model the Ca sorption as well as the Sr and Cs sorption on Ca-smectite with only one set of site retention parameters. Note that the $K^{i*}_{2H+/Ca2+}$ and $K^{i*}_{2H+/Sr2+}$ values obtained for Xe, Xf and Xg were comparable, which is consistent with the similar chemical behaviors of Ca and Sr. For Cs, the contribution of the sites Xf and Xg were too low to be quantified with good accuracy.

Table 1

Site capacities CE_i and selectivity coefficients $K^{i*}_{2H+/Ca2+}$, $K^{i*}_{2H+/Sr2+}$ and $K^{i*}_{H+/Cs+}$ of Ca-illite and Ca-smectite determined and used in this study.

	Sites	CE_i (eq/kg)	$\log K^{*i}_{2H^+/Ca^{2+}}$	$\log K^{*i}_{2H^+/Sr^{2+}}$	$\log K^{*i}_{H^+/Cs^{2+}}$
Illite	Xh	0.001	-0.403 ± 1.977	1.700 ± 1.823	5.679 ± 1.004
	Xa	0.131	-2.166 ± 0.073	-2.435 ± 0.640	0.852 ± 0.512
	Xb	0.043	-4.311 ± 0.216	-3.685 ± 0.367	-4.909 ± ∞
	Xc	0.074	-11.745 ± 0.205	-11.250 ± 0.713	-13.853 ± ∞
Smectite	Xj	0.0001	1.459 ± 0.577	-	3.849 ± 0.270
	Xe	0.387	-0.491 ± 0.486	-0.310 ± 0.028	0.648 ± 0.067
	Xf	0.361	-4.352 ± 0.032	-4.475 ± 0.081	-7.797 ± ∞
	Xg	0.139	-14.837 ± 0.063	-14.778 ± 0.201	-13.502 ± ∞

4.2. Modeling Sr and Cs sorption data on clayey sandstone

4.2.1. Sorption experiment

Sr and Cs sorption and desorption isotherms vs. concentration (Fig. 7 & 8) were acquired on batch experiments performed with the CS < 25 µm fraction equilibrated in a 0.01M $CaCl_2$ background solution at pH 6.4. In these cases, Sr and Cs showed two distinct behaviors. For Sr, $\log(K_d)$ appeared to be constant at a value of 1.30 between concentrations 10^{-7} and 10^{-3}M which means that the sorption tended to increase regularly with the concentration, except up to 10^{-3} M when the total exchange capacity began to be reached. On the contrary, Cs sorption depended on its concentration with $\log(K_d)$ decreasing irregularly from 4.70 at low concentration (10^{-7}M) to 0.70 at 10^{-1}M when the total

exchange capacity was reached. The high sorption at low Cs concentration ($<10^{-5}$M) was consistent with the contribution of low-capacity sites having a high affinity for Cs on illite (Poinssot et al., 1999; Missana et al., 2014b). In both case, the desorption curve was superimposed on the sorption curve, proving that Sr and Cs sorption reactions on this material (natural illite and smectite mixture) were reversible under the employed experimental conditions. According to these experiments, no sorption or desorption kinetics with shorter contact times could be evidenced, but some authors pointed out a fast (24 h) Sr and Cs sorption on clay mineral by ion exchange mechanisms (Torstenfelt et al., 1982; Hsu et al., 1994; Galambos et al., 2013). Chemical equilibrium was indeed reached in 6 days, in our case.

These results are consistent with the Sr sorption reversibility observed previously on illite and smectite (this study; Axe et al., 1998; Chen and Hayes, 1999; Wang and Staunton, 2005).

However, the reversibility of Cs sorption on illite remains controverted. At first, the non-reversibility of Cs sorption observed by some authors can be attributed to differences between the chemical conditions of their adsorption and desorption. Among the authors respecting the same chemical conditions for their sorption/desorption experiments, some of them did not observe this reversibility after 2h (Staunton and Roubaud, 1997), 24h (Bellenger and Staunton, 2008) and even 12 days of contact time (Comans et al., 1991). They attributed this irreversibility to high-affinity sites acting to retain Cs by collapsing the interlayer space (Sawhney, 1972; Brouwer et al., 1983). Nonetheless, this non-reversibility was not evident since desorption phenomenon seem to depend both on the experimental time, the nature of the competing cations and the ionic strength of the solution (Koning et al., 2004). Therefore, Gorgeon (1994) observed the reversibility of Cs sorption on illite in a high ionic strength (1M NaCl) solution after a few hours. Unfortunately, the reversibility of Cs sorption on Ca-illite (sorption data used in this study) was not investigated by Missana et al. (2014b), wherefore we cannot conclude on the reversibility of Cs sorption on illite at lower ionic strength. Nevertheless, the reversibility of the Cs sorption observed in our experimental results was verified despite the presence of illite contained in equivalent abundance to smectite in the clayey sandstone. This reversibility supports the pertinence of applying an ion-exchange model based on the mass action law, as addressed in the multi-site ion exchanger model, to interpret the experimental data.

4.2.2. Modeling by the component additivity approach

The component additivity approach to simulate Sr and Cs sorption on a clayey sandstone CS, is also based on our capability to determine with good accuracy the relative contributions of illite and smectite in the total CS sorption properties. XRD quantification denoted a relative abundance of illite (27%) and of smectite (26%) in the < 25 µm fraction of CS. They contributed respectively to 0.068 eq/kg and 0.233 eq/kg, corresponding to 21 % and 73 % of the CEC (i.e., 0.326 eq/kg). Therefore, the ion exchanger was assimilated to 27 % of illite associated to 26 % of smectite, corresponding to a total site capacity around 0.301 eq/kg; slightly below the total CEC, given that kaolinite and chlorite contributions were neglected. The exchanger site capacity was defined according to Eq. 8. The modeling input parameters are listed in Table 1 and simulations were carried out without adjusted parameters. The modeling outcomes were compared with experimental data, and envelope curves taking into account the biggest uncertainties of the selectivity coefficients are presented in Fig. 7 & 8. The Sr sorption may have been slightly underestimated since the contribution of kaolinite and chlorite was neglected. However, the envelope curves taking into account the K_d value uncertainties showed that the sorption curves provided by the multi-site ion exchanger model were overall in good agreement with the experimental Sr and Cs sorption data on the natural sediment. Indeed, the multi-site ion exchanger model was able to take into account the variations in Sr and Cs concentration and the competition with Ca in retention processes, without any adjustment of the parameters.

We have thus demonstrated that the multi-site ion exchanger model integrated in a component additivity approach was pertinent for predicting Sr and Cs sorption on natural clayey sandstone. This also confirms the robustness of the sorption database established in this study.

5. Conclusions

Considering that clay minerals behave as multi-site ion-exchangers, a database compiling the retention properties of Ca-illite and Ca-smectite towards Sr and Cs was created and was used to

predict the sorption of Sr and Cs on a natural clayey sediment. The good agreement between the experimental results and the simulations was the first step to demonstrating the additivity of the sorption properties of the mineralogical phases in a natural material defined as a mixture of these phases. The confirmation of these results under various chemical conditions would support the predictive character of the multi-site ion exchange model. Other experiments of reactive transport carried out in sediment columns are currently in progess and already confirm the predictive character of this approach in the case of Sr (Wissocq et al., in prep).

Acknowledgments

This work was financially supported by CEA. We thank P. Fichet for the ICP-MS analysis, B. Siroux for his contribution to the elaboration of the database, and ERM for the XRD-quantification of the mineral phases.

References

Altmann, S., Aertsens, M., Appelo, T., Bruggeman, C., Gaboreau, S., Glaus, M., Jacquier, P., Kupcik, T., Maes, N., Montoya, V., Rabung, T., Robinet, J-C., Savoye, S., Schaefer, T., Tournassat, C., Van Laer, L., Van Loon, L., 2014. Processes of cation migration in clayrocks, CatClay Final Scientific Report D1.6.

Axe, L., Bunker, G.B., Anderson, P.R., Tyson, T.A., 1998. An XAFS analysis of strontium at the hydrous ferric oxide surface. J. Colloids Interf. Sci. 199, 44-52.

Baeyens, B., Bradbury, M.H., 1997. A mechanistic description of Ni and Zn sorption on Na-montmorillonite. Part I: Titration and sorption measurements. J. Contam. Hydrol. 27, 199-222.

Baeyens, B., Bradbury, M.H., 2004. Cation exchange capacity measurements on illite using the sodium and cesium isotope dilution technique: effects of the index cation, electrolyte concentration and competition: modeling. Clay Clay Min. 52, 421-431.

Beek, J., Bolt, G.H., Bruggenwert, M.G.M., Haan, F.A.M., Harmsen, K., Kamphorst, A., Van Riemsdijk, W.H., Brinkman, R., Cleary, R.W., Van Genuchten, M.T., Cremers, A., Maes, A. B., 1979. Physico-chemical models. In: Bolt, G.H. (Ed.), Soil Chemistry. Elsevier Scientific Publishing Company, Amsterdam, 141–203.

Bellenger, J-P., Staunton, S., 2008. Adsorption and desorption of ^{85}Sr and ^{137}Cs on reference minerals, with and without inorganic and organic surface coatings. J. Environ. Radioact 99, p. 831-840.

Bolt, G.H., De Boodt, M.F., Hayes, H.B., McBride, M.B., 1991. Interactions at the Soil Colloid – Soil Solution Interface. Kluwer Academic Publishers, Dordrecht.

Bradbury, M.H., Baeyens, B., 1999. Modelling the sorption of Zn and Ni on Ca-montmorillonite. Geochim. Cosmochim. Acta, 63, 325-336.

Bradbury, M.H., Baeyens, B., 2000. A generalised model for the concentration dependent uptake of caesium by argillaceous rocks. J. Contam. Hydrol. 42, 141–163.

Brouwer, E., Baeyens, B., Maes, A., Cremers, A., 1983. Cesium and rubidium ion equilibriums in illite clay. The J. Phys. Chem. 87, p. 1213-1219.

Chen, C.-C., Hayes, K.F., 1999. X-ray absorption spectroscopy investigation of aqueous Co(II) and Sr(II) sorption at clayewater interfaces. Geochim. Cosmochim. Acta 19/20, 3205-3215.

Comans, RNJ, Hailer, M, de Preter, R., 1991. Sorption of cesium on illite: Non-equilibrium behaviour and reversibility. Geochim. Cosmochim. Acta 55, p. 433-440.

Davies, C.W, 1938. The Extent of Dissociation of Salts in Water. Part VIII. An Equation for the Mean Ionic Activity Coefficient of an Electrolyte in Water, and a Revision of the Dissociation Constants of Some Sulphates. J. Chem Soc. PT.2, 2093–2098.

Davis, J.A., Coston, J.A., Kent, D.B., Fuller, C.C., 1998. Application of the surface complexation concept to complex mineral assemblages. Environ. Sci. Technol. 32, 2820–2828.

Davis, J.A., Meece, D.E., Kohler, M., Curtis, G.P., 2004. Approaches to surface complexation modeling of Uranium (VI) adsorption on aquifer sediments. Geochim. Cosmochim. Acta 68, 3621–3641.

Dong, W.,Tokunaga, T.K., Davis, J.A., Wan, J., 2012. Uranium (VI) adsorption and surface complexation modeling onto background sediments from the F-Area Savannah River Site. Environ. Sci. Technol. 46, 1565–1571.

El Aamrani, F.Z., Duro, L., De Pablo, J., Bruno, J., 2002. Experimental study and modeling of the sorption of uranium(VI) onto olivine-rock. Appl. Geochem. 17, 399–408.

Gabis, V. ,1958. Etude préliminaire des argiles oligocènes du Puy-en-Velay (Haute-Loire). Bull. Soc. Franc. Minéral. Cristallog. 81, 183–185.

Galambos, M., Krajnak, A., Rosskopfova, O., Viglasova, E., R. Adamcova, R., Rajec, P., 2013. Adsorption equilibrium and kinetic studies of strontium on Mg-bentonite, Fe-bentonite and illite/smectite. J. Radioanal. Nucl. Chem. 298, 1031–1040.

Gaucher, E., 1998. Interactions eaux-argiles : étude expérimentale. Thesis, Univ. Paris 7, France.

Guillaume, D., 2002. Etude expérimentale du système fer-smectite en solution à 80 et 300°C". Thesis, Univ. Henri Poincaré, Nancy.

Gorgeon, L., 1994. Contribution à la modélisation physico-chimique de la rétention de radioéléments à vie longue par des matériaux argileux. Thesis, Univ. Paris 6, France, 1-202.

Hsu, C-N., Liu, D-C., Chuang, C-L., 1994. Equilibrium and Kinetic Sorption Behaviors of Cesium and Strontium in Soils. Appl. Radiat. Isot. 45, 981-985.

Jackson, M.L., 1963. Interlayering of expansible layer silicates in soils by chemical weathering. Clay Clay Min. 11, 29-46.

Jacquier, P., Ly, J., Beaucaire, C., 2004. The ion-exchange properties of the Tournemire argilite I. Study of the H, Na, K, Cs, Ca and Mg behaviour. Appl. Clay Sci. 26, 163–170.

Koning, A., Comans, R.N.J., 2004. Reversibility of radiocaesium sorption on illite. Geochim. Cosmochim. Acta, 68, 13, 2815–2823,

Kurosawa, S., James, S.C., Yui, M., Ibaraki, M., 2006. Model analysis of the colloid and radionuclide retardation experiment at the Grimsel Test Site. J. Colloids Interf. Sci. 298, 467–475.

Landry, C.J., Koretsky, C.M., Lund, T.J., Schaller, M., Das, S., 2009. Surface complexation modeling of Co(II) adsorption on mixtures of hydrous ferric oxide, quartz and kaolinite. Geochim. Cosmochim. Acta 73, 3723-3737.

Ly, J., Pitsch, H., Stammose, D., 1991. Description of actinides sorption onto clays by ion-exchange mechanism. Migration 91, Jerez de la Frontera, Espagne.

Michot, L., Bihannic, I. Porsch, K., Maddi, S., Baravian, C., Mougel, J., Levitz, P., 2004. Phase diagrams of Wyoming Na-montmorillonite clay. Influence of particle anisotropy. Langmuir 20, 10829–10837.

Missana, T, Garcia-Gutierrez, M, Alonso, U., 2004. Kinetics and irreversibility of cesium and uranium sorption onto bentonite colloids in a deep granitic environment. Appl. Clay Sci. 26, 137–150.

Missana, T., Benedicto, A., Garcia-Gutierrez, M., Alonso U., 2014a. Modeling cesium retention onto Na-, K- and Ca-smectite: Effects of ionic strength, exchange and competing cations on the determination of selectivity coefficients. Geochim. Cosmochim. Acta 128, 266-277.

Missana, T., Garcia-Gutierrez, M., Alonso U., 2014b. Modelling of Cs sorption in natural mixed-clays and the effects of ion competition. Applied Geochem. 49, p. 95-102.

Motellier, S., Ly, J., Gorgeon, L., Charles, Y., Hainos, D., Meier, P., Page, J., 2003. Modelling of the ion-exchange properties and indirect determination of the interstitial water composition of an argillaceous rock. Application to the Callovo-Oxfordian low-water-content formation. Appl. Geochem. 18, 1517–1530.

Nolin, D., 1997. Rétention de radioéléments à vie longue par des matériaux argileux. Influence d'anions contenus dans les eaux naturelles. Thesis, Univ. Paris 6, France, 1–219.

Payne, T.E., Davis, A.D., Ochs, M., Olin, M., Tweed, C.J., 2004. Uranium adsorption on weathered schist–intercomparison of modeling approaches. Radiochim. Acta 92, 651–661.

Peynet, V., 2003. Rétention d'actinide et de produits de fission par des phases solides polyminérales. Thesis, Univ. Paris 6, France, 1–256.

Poinssot, C, Baeyens, B, Bradbury, M.H., 1999. Experimental studies of Cs, Sr, Ni and Eu sorption on Na-illite and the modelling of Cs sorption. Nagra Technical Report 99-04.

Rafferty, P., Shiao, S.Y., Binz, C.M., Meyer, R.E., 1981. Adsorption of Sr(II) on clay minerals: effects of salt concentration, loading and pH. J. Inorg. Nucl. Chem. 43, 797-805.

Reich, T.J., Das, S., M., Koretsky, C.M., Lund, T.J., Landry, C.J., 2010; Surface complexation modeling of Pb(II) adsorption on mixtures of hydrous ferric oxide, quartz and kaolinite. Chem. Geol. 275, 262-271.

Reinoso-Maset, E., Ly, J., 2014. Study of major ions sorption equilibria to characterize the ion exchange properties of kaolinite. J. Chem. Eng. Data, 59 (12), 4000-4009.

Reinoso-Maset, E., Ly, J., 2016. Study of uranium(VI) and radium(II) sorption at trace level on kaolinite using a multisite ion exchange model. J. Environ. Radioact. 157, 136–148.

Robin, V., Tertre, E., Beaufort, D., Regnault, O., Sardini, P., Descostes, M., 2015. Ion exchange reactions of major inorganic cations (H+ , Na+ , Ca2+, Mg2+ and K+) on beidellite: Experimental results and new thermodynamic database. Toward a better prediction of contaminant mobility in natural environments. Applied Geochemistry 59, 74–84.

Sauzéat, E., Villiéras, F., François, M., Pelletier, M., Barrès, O., Yvon, J., Guillaume, D., Dubessy, J., Peiffert, C., Mosser-Ruck, R., Cathelineau, M., 2000. Caractérisation minéralogique, cristallochimique et texturale de l'argile MX80. Rapport ANDRA C RP 0LEM 01-001.

Savoye, S.; Beaucaire, C.; Fayette, A.; Herbette, M.; Coelho, D., 2012. Mobility of cesium through the callovo-oxfordian claystones under partially saturated conditions. Environ. Sci. Technol. 46 (5), 2633−2641.

Sawhney, B.L., 1972. Selective sorption and fixation of cations by clay minerals. Clay Clay Min. 20, 93-100.

Schaller, M., Koretsky, C.M., Lund, T.J., Landry, C.J., 2009. Surface complexation modeling of Cd(II) adsorption on mixtures of hydrous ferric oxide, quartz and kaolinite. J. Colloids Interf. Sci. 339, 302–309.

Siroux, B., Beaucaire, C., Benedetti, M.F., Reiller, P.E., 2017. Adsorption of strontium and cesium onto a Na-MX80 bentonite: experiments and building of a coherent thermodynamic modelling. Applied Geochem. (submitted).

Staunton, S., Roubaud, M., 1997. Sorption of ^{137}Cs on montmorillonite and illite: effect of charge compensating cation, ionic strength, concentration of Cs, K and fulvic acid. Clay Clay Min. 45(2), 251-260.

Steefel, C.I., Caroll, S., Zhao, P., Roberts, S., 2003. Cesium migration in Hanford sediment: a multisite cation exchange model based on laboratory transport experiments. J. Contam. Hydrol. 67, 219–246.

Tertre, E., Hofmann, A., Berger, G., 2008. Rare earth element sorption by basaltic rock: experimental data and modeling results using the ‘‘generalised composite approach’’. Geochim. Cosmochim. Acta 72, 1043–1056.

Tertre, E., Beaucaire, C., Coreau, C., Juery, A., 2009. Modelling Zn(II) sorption onto clayey sediments using a multi-site ion-exchange model. Applied Geochem. 24, 1852–1861.

Torstenfelt B., Andersson K., Allard B., 1982. Sorption of cesium and strontium on rocks and minerals. Chem. Geol. 36, 123-137.

Tournassat, C., Ferrage, E., Poinsignon, C., Charlet, L., 2004. The titration of clay minerals. Part II. Structure based model and implications for clay reactivity. J. Colloids Interf. Sci. 273, 234-246.

Vandenhove, H., Van Hees, M., Wouters, K., Wannijn, J., 2007. Can we predict uranium bioavailability based on soil parameters? Part 1: effect of soil parameters on soil solutions uranium concentration. Environ. Pollut. 145, 587–595.

Van Olphen, H., Fripat, J.J., 1979. Data Handbook for Clay Materials and Other Non-metallic Minerals. Pergamon, New-York, 346 pp.

Voegelin, A., Vulava, V.M., Huhnen, F., Kretzschmar, R., 2000. Multicomponent transport of major cations predicted from binary adsorption experiments. J. Contam. Hydrol. 46, 319–338.

Vulava, V.M., Kretzschmar, R., Rusch, U., Grolimund, D., Westall, J., Borkovec, M., 2000. Cation competition in a natural subsurface material: modelling of sorption equilibria. Environ. Sci. Technol. 34, 2149–2155.

Vulava, V.M., Kretzschmar, R., Barmettler, K., Voegelin, A., 2002. Cation competition in a natural subsurface material: prediction of transport behavior. Water Resour. Res. 38, http://onlinelibrary.wiley.com/doi/10.1029/2001WR000262/epdf

Wahlberg, J.S., Fishman M.J., 1962. Adsorption on cesium on clay minerals. Geological survey bulletin 1140-A.

Wahlberg, J.S., Baker, J.H., Vernon, R.W., Dewar, R.S., 1965. Exchange adsorption of strontium on clay minerals. Geological survey bulletin 1140-C.

Wang, G., Staunton, S., 2005. Evolution of Sr distribution coefficient as a function of time, incubation conditions and measurement technique. J. Environ. Radioact. 81, 173-185.

Wissocq, A., Beaucaire, C., Latrille, C., 2017. Ca and Sr sorption on Ca-illite: experimental study and modelling. Procedia Earth and Planetary Science 17**,** 662-665.

Figures caption:

Figure 1. Na (I=0.02M) and Ca (I=0.02M) saturation curves on smectite (Nolin, 1997; Peynet et al., 2003) and modeling (full line)

Figure 2. Logarithm of the Sr distribution coefficient vs. the Sr concentration at equilibrium (pH=6.5 (here, blue diamonds for sorption and yellow for desorption)) and pH=7 (Wahlberg et al. (1965) (orange dots)) on Ca-illite (I=0.03M) and the modeling outcome (red line). Contribution of the high-capacity sites Xa, Xb and Xc (violet, green and orange dashed lines) and the low-capacity site (blue dashed line).

Figure 3. Logarithm of the Cs distribution coefficient vs. the Cs concentration at equilibrium (pH=7) on Ca-illite (I=0.1M) (Missana et al., 2014b) and the modeling outcome (red line). Contribution of the high-capacity site Xa (violet dashed line) and the low-capacity site Xh (blue dashed line).

Figure 4. Logarithm of the Sr distribution coefficient vs. pH (a) ($[Sr]_i = 10^{-7}$M) and vs. the Sr concentration at equilibrium on Ca-smectite (I=0.03M) (pH=7.5 (here, blue diamonds for sorption and yellow for desorption) and pH=7 (Wahlberg et al. (1965) (orange dots)) and (b) the modeling outcome (red line). Contribution of the high-capacity sites Xe, Xf and Xg (violet, green and orange dashed lines).

Figure 5. Logarithm of the distribution coefficient of Cs vs. pH (a) ($[Cs]_i = 10^{-7}$M) and vs. the Cs concentration at equilibrium on Ca-smectite as well as the modeling (pH=4 and I=0.03M (here, blue diamonds for sorption and yellow for desorption), pH=7 and I=0.03M (Wahlberg and Fishman (1962) (orange dots)) and pH 6.5 and I=0.1M (Missana et al., 2014a) (green squares)) (b). Contribution of the high-capacity site Xe (violet dashed line) and the low-capacity site Xj (blue dashed line).

Figure 6. Logarithm of the adsorbed concentration of Sr and Cs vs. concentration at equilibrium on Ca-illite and Ca-smectite (I=0.03M)

Figure 7. Logarithm of the distribution coefficient of Sr vs. the Sr concentration at equilibrium on clayey sandstone (I=0.03M, pH 6.4) and modeling.

Figure 8. Logarithm of the distribution coefficient of Cs vs. the Cs concentration at equilibrium on clayey sandstone (I=0.03M, pH 6.4) and modeling.

Table captions:

Table 1: Site capacities CE_i and selectivity coefficients $K^{i*}_{2H+/Ca2+}$, $K^{i*}_{2H+/Sr2+}$ and $K^{i*}_{H+/Cs+}$ of Ca-illite and Ca-smectite determined and used in this study.

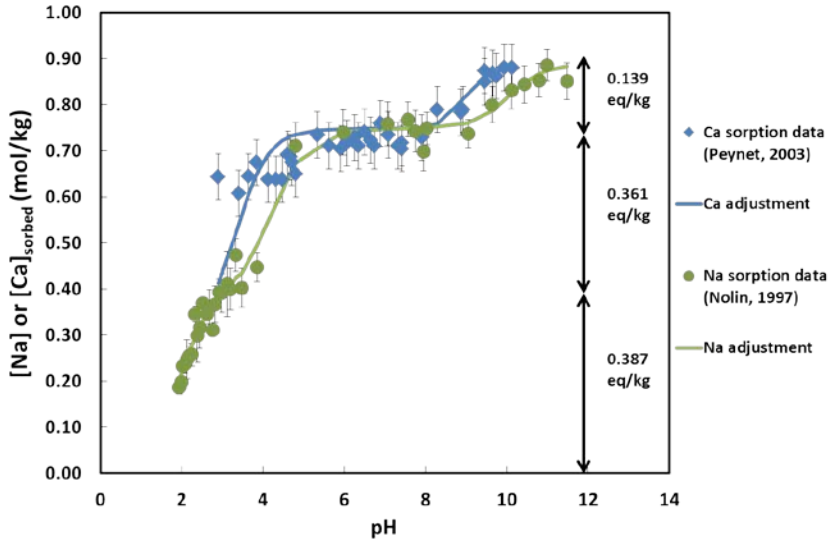

Fig. 1. Na (I=0.02M) and Ca (I=0.02M) saturation curves on smectite (Nolin, 1997; Peynet et al., 2003) and modeling (full line)

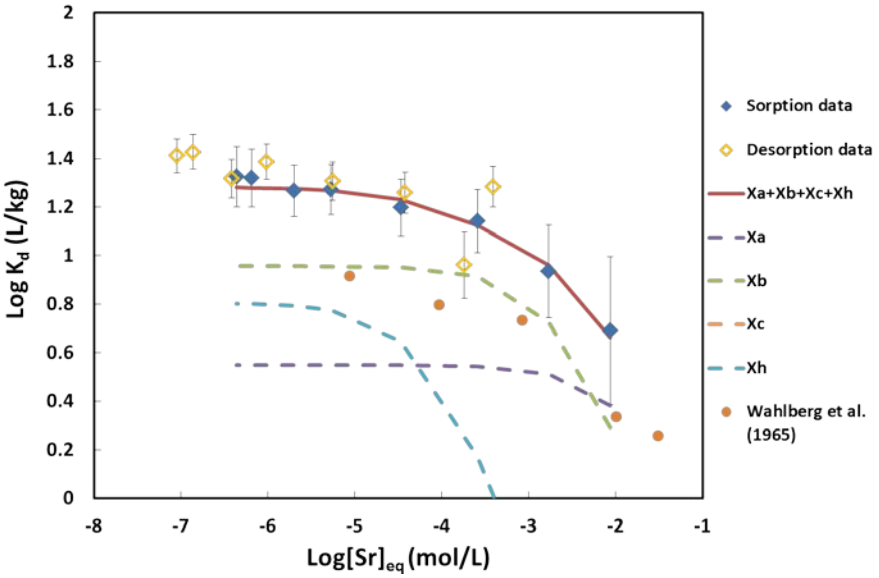

Fig. 2. Logarithm of the Sr distribution coefficient vs. the Sr concentration at equilibrium (pH=6.5 (here, blue diamonds for sorption and yellow for desorption)) and pH=7 (Wahlberg et al. (1965) (orange dots)) on Ca-illite (I=0.03M) and the modeling outcome (red line). Contribution of the high-capacity sites Xa, Xb and Xc (violet, green and orange dashed lines) and the low-capacity site (blue dashed line).

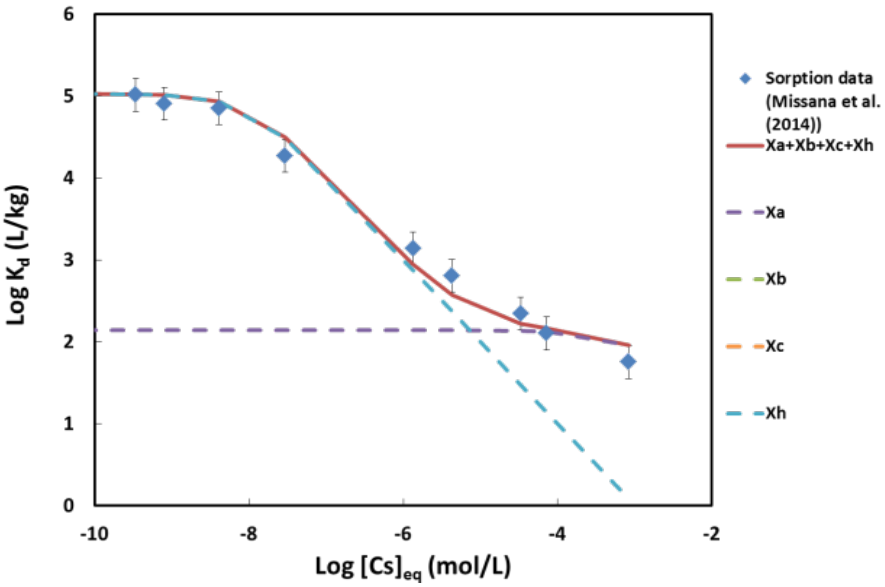

Fig. 3. Logarithm of the Cs distribution coefficient vs. the Cs concentration at equilibrium (pH=7) on Ca-illite (I=0.1M) (Missana et al., 2014b) and the modeling outcome (red line). Contribution of the high-capacity site Xa (violet dashed line) and the low-capacity site Xh (blue dashed line).

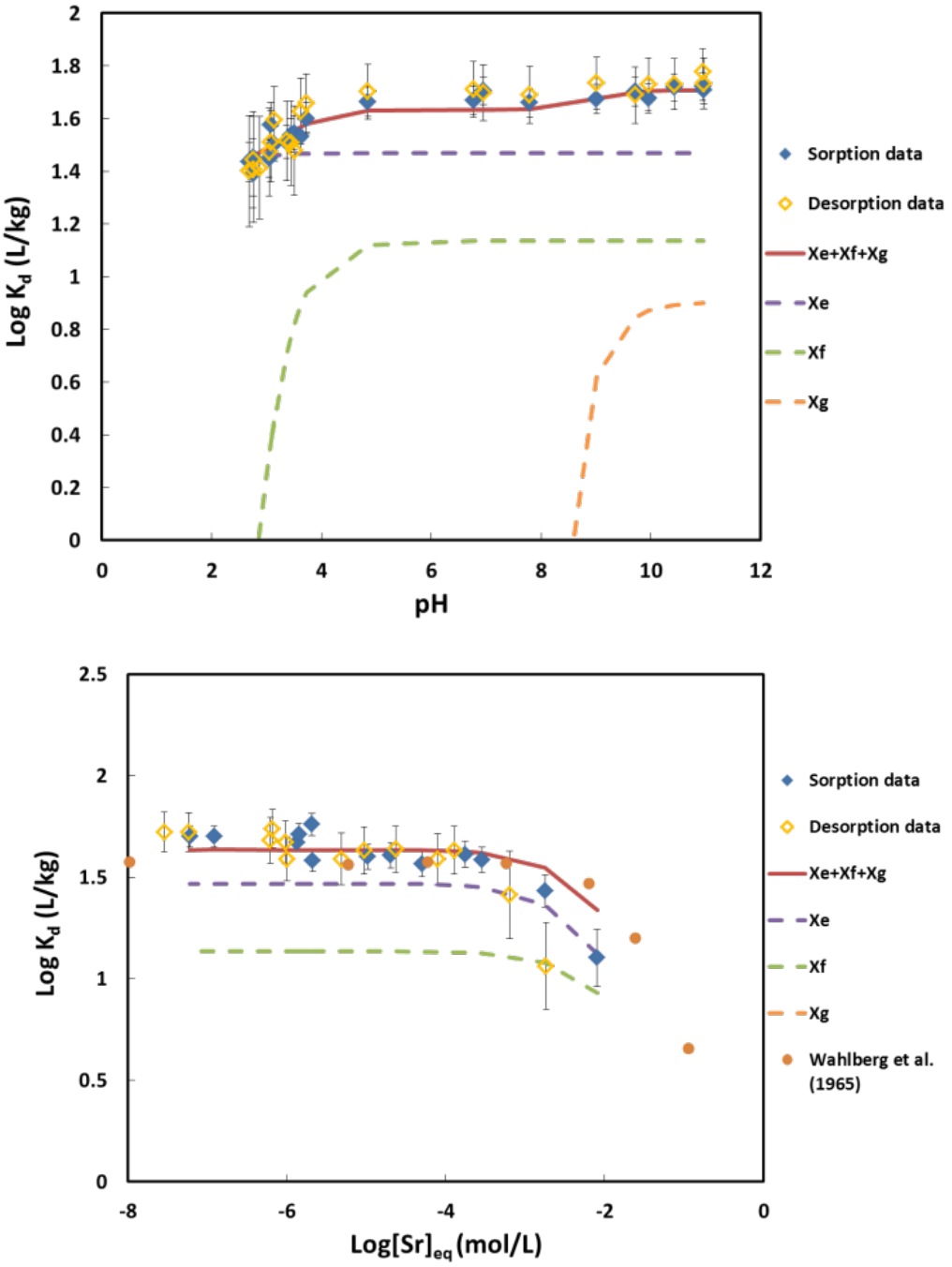

Fig. 4. (a) and (b) Logarithm of the Sr distribution coefficient vs. pH (a) ($[Sr]_i = 10^{-7}$M) and vs. the Sr concentration at equilibrium on Ca-smectite (I=0.03M) (pH=7.5 (here, blue diamonds for sorption and yellow for desorption) and pH=7 (Wahlberg et al. (1965) (orange dots)) and (b) the modeling outcome (red line). Contribution of the high-capacity sites Xe, Xf and Xg (violet, green and orange dashed lines).

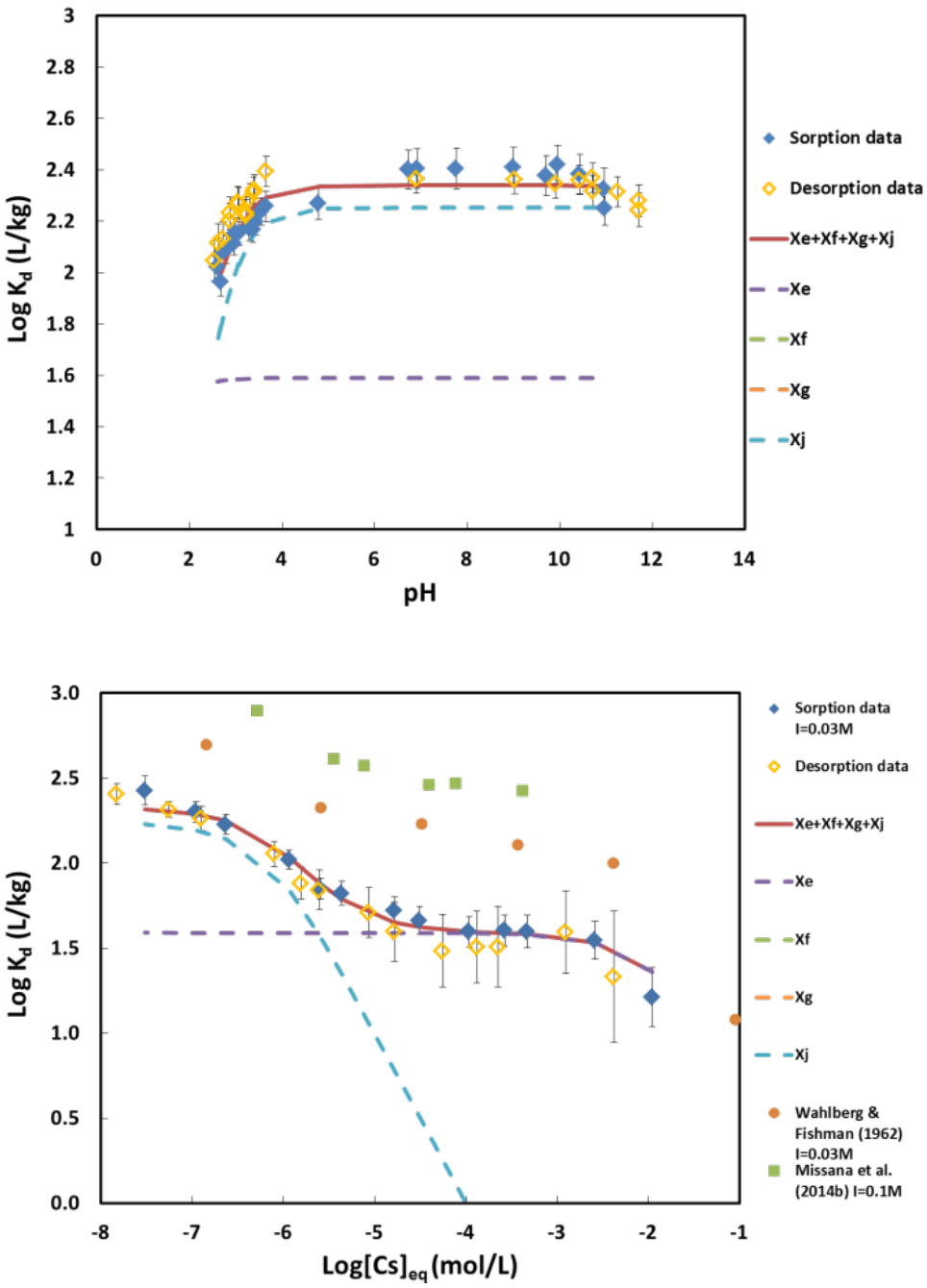

Fig. 5. (a) and (b) Logarithm of the distribution coefficient of Cs vs. pH (a) ($[Cs]_i = 10^{-7}$M) and vs. the Cs concentration at equilibrium on Ca-smectite as well as the modeling (pH=4 and I=0.03M (here, blue diamonds for sorption and yellow for desorption), pH=7 and I=0.03M (Wahlberg and Fishman (1962) (orange dots)) and pH 6.5 and I=0.1M (Missana et al., 2014a) (green squares)) (b). Contribution of the high-capacity site Xe (violet dashed line) and the low-capacity site Xj (blue dashed line).

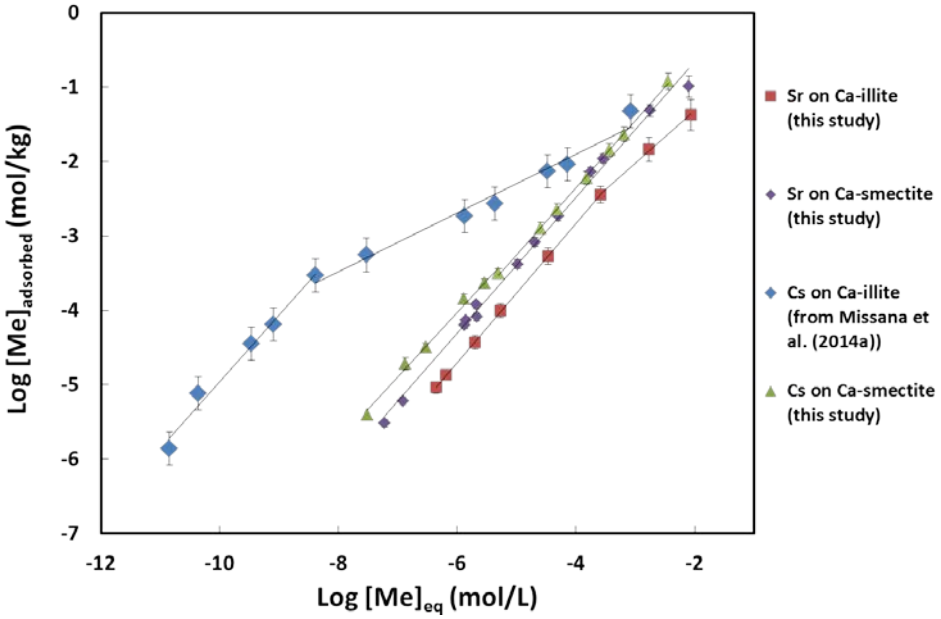

Fig. 6. Logarithm of the adsorbed concentration of Sr and Cs vs. concentration at equilibrium on Ca-illite and Ca-smectite (I=0.03M)

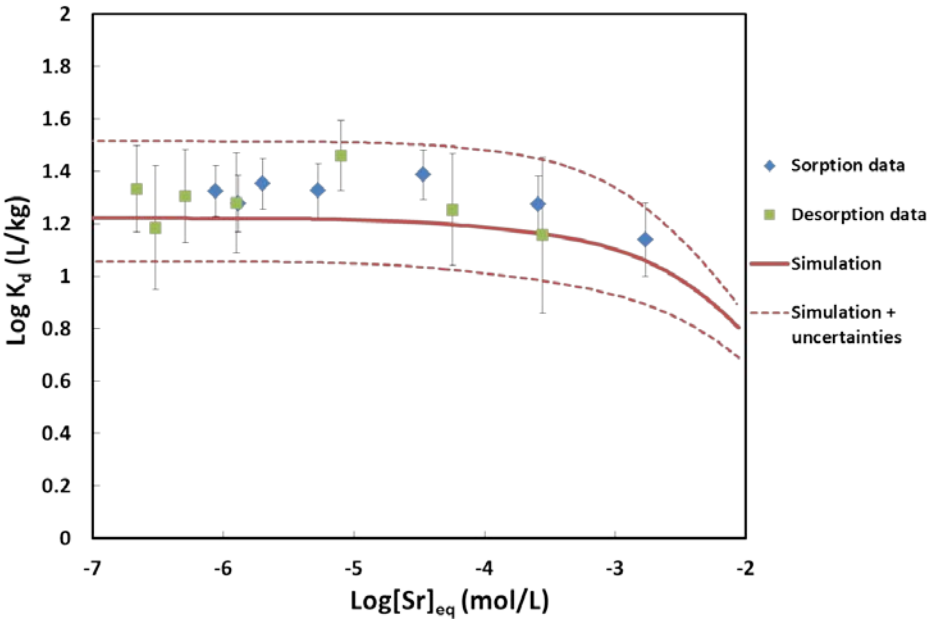

Fig. 7. Logarithm of the distribution coefficient of Sr vs. the Sr concentration at equilibrium on clayey sandstone (I=0.03M, pH 6.4) and modeling.

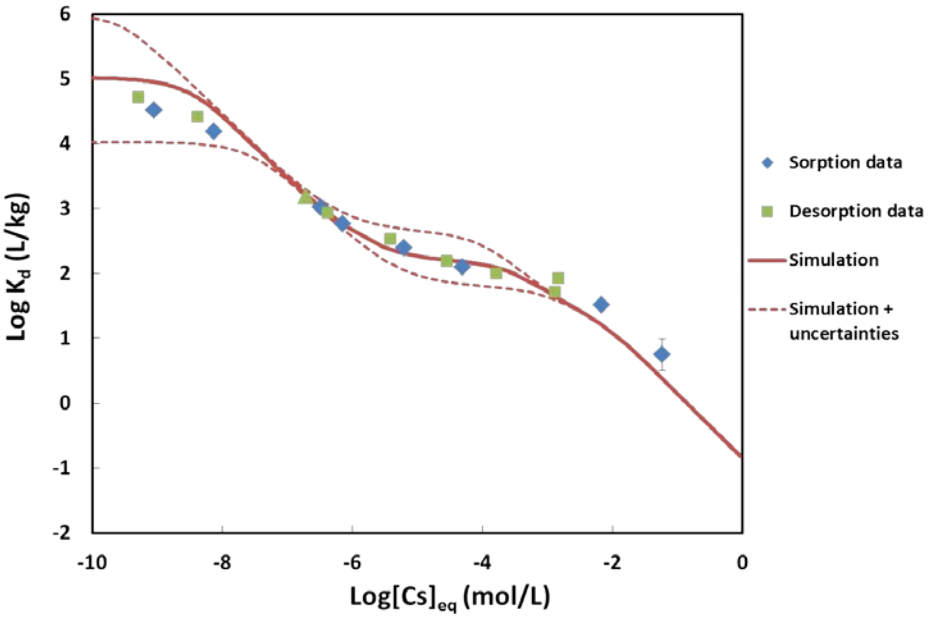

Fig. 8. Logarithm of the distribution coefficient of Cs vs. the Cs concentration at equilibrium on clayey sandstone (I=0.03M, pH 6.4) and modeling.

Appendix 1

The results of the new adjustment of the Ca saturation curve and the Sr sorption curve vs. pH (Wissocq et al., 2017) with the site capacities Xa, Xb, Xc and Xh (0.131, 0.043, 0.074 and 0.001 eq/kg) is presented in the two figures below.

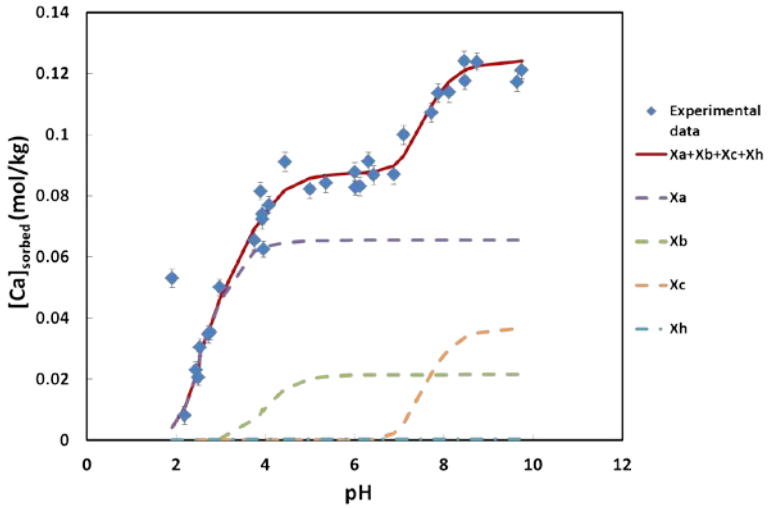

Fig. A1. Ca saturation curve on Ca-illite (I=0.03M) and modeling.

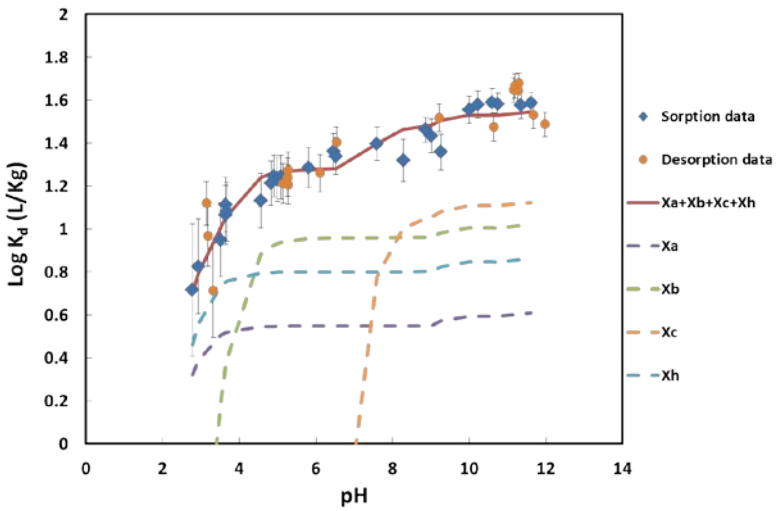

Fig A2. Logarithm of the distribution coefficient of Sr vs. pH on Ca-illite (I=0.03M; $[Sr]_i = 10^{-7}$M) and modeling (Wissocq et al., 2017).

Appendix 2

The concentration of adsorbed Ca^{2+} in competition with Na^{+} is given by the following equation:

$$[(X_i^-)_2 - Ca^{2+}] = \frac{1}{8}(4CE_i + E^2F - \sqrt{E^4F^2 + 8CE_iE^2F})$$

with $E = 1 + \frac{K^i_{H^+/Na^+}\ \gamma_{Na^+}\ [Na^+]}{10^{-pH}}$ and $F = \frac{10^{-2pH}}{K^i_{2H^+/Ca^{2+}}\ \gamma_{Ca^{2+}}\ [Ca^{2+}]}$

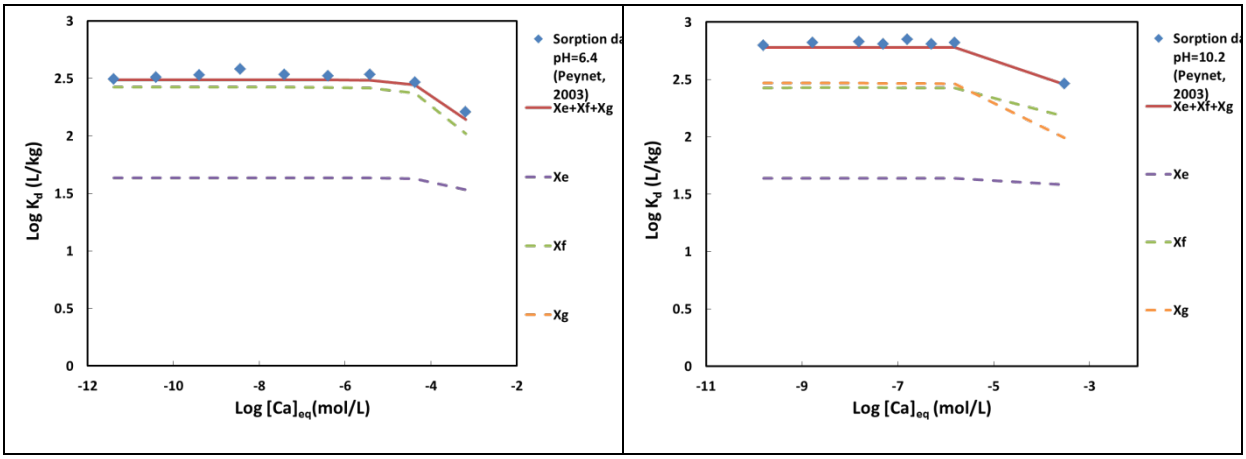

Fig. A3. Logarithm of the distribution coefficient of Ca vs. Ca concentration at equilibrium on Na-smectite (I=0.05M) at pH=6.4 (a) and pH=10.2 (b) (Peynet et al., 2003) and modeling.

Table A1

Site capacities CE_i and selectivity coefficients $K^{i*}_{H+/Na+}$ for Na-smectite used in this study (Siroux et al., 2017).

Sites	CE_i (eq/kg)	Log $K^{*i}_{H^+/Na^+}$
Xe	0.387	-0.263 ± 0.036
Xf	0.361	-2.619 ± 0.085
Xg	0.139	-8.454 ± 0.184